In vitro osteogenesis on a highly bioactive glass-ceramic (Biosilicate®)

João Moura,[1] Lucas Novaes Teixeira,[1] Christian Ravagnani,[2] Oscar Peitl,[2] Edgar Dutra Zanotto,[2] Márcio Mateus Beloti,[1] Heitor Panzeri,[1] Adalberto Luiz Rosa,[1] Paulo Tambasco de Oliveira[1]

[1]*Cell Culture Laboratory, Faculty of Dentistry of Ribeirão Preto, University of São Paulo, Av. do Café, s/n, CEP 14040-904, Ribeirão Preto, São Paulo, Brazil*

[2]*Vitreous Materials Laboratory, Department of Materials Engineering, Federal University of São Carlos, CP. 676, CEP 13565-905, São Carlos, São Paulo, Brazil*

Received 21 April 2006; revised 30 August 2006; accepted 1 November 2006
Published online 20 February 2007 in Wiley InterScience (www.interscience.wiley.com). DOI: 10.1002/jbm.a.31165

Abstract: One of the strategies to improve the mechanical performance of bioactive glasses for load-bearing implant devices has been the development of glass-ceramic materials. The present study aimed to evaluate the effect of a highly bioactive, fully-crystallized glass-ceramic (Biosilicate®) of the system P_2O_5–Na_2O–CaO–SiO_2 on various key parameters of *in vitro* osteogenesis. Surface characterization was carried out by scanning electron microscopy and Fourier transform infrared spectroscopy. Osteogenic cells were obtained by enzymatic digestion of newborn rat calvarial bone and by growing on Biosilicate® discs and on control bioactive glass surfaces (Biosilicate® parent glass and Bioglass® 45S5) for periods of up to 17 days. All materials developed an apatite layer in simulated body fluid for 24 h. Additionally, as early as 12 h under culture conditions and in the absence of cells, all surfaces developed a layer of silica-gel that was gradually covered by amorphous calcium phosphate deposits, which remained amorphous up to 72 h. During the proliferative phase of osteogenic cultures, the majority of cells exhibited disassembly of the actin cytoskeleton, whereas reassembly of actin stress fibers took place only in areas of cell multilayering by day 5. Although no significant differences were detected in terms of total protein content and alkaline phosphatase activity at days 11 and 17, Biosilicate® supported significantly larger areas of calcified matrix at day 17. The results indicate that full crystallization of bioactive glasses in a range of compositions of the system P_2O_5–Na_2O–CaO–SiO_2 may promote enhancement of *in vitro* bone-like tissue formation in an osteogenic cell culture system. © 2007 Wiley Periodicals, Inc. J Biomed Mater Res 82A: 545–557, 2007

Key words: bioactive glass; crystallization; glass-ceramic; bioactivity; osteogenesis; cell culture

INTRODUCTION

The bioactive glass Bioglass® 45S5 has been known for many years as the bioactive material with the highest bioactivity index, which is defined as the inverse of the time required for 50% of the surface of the material to be intimately bound to the bone.[1] It has been demonstrated that Bioglass® 45S5 affects osteoblast activities that ultimately result in enhanced bone formation both *in vitro* and *in vivo*.[2] Indeed, at least seven families of genes are upregulated when primary human osteoblasts are exposed to the ionic dissolution products of bioactive glasses, including genes that encode proteins associated with osteoblast proliferation and differentiation.[3–5] Despite its beneficial effects on bone healing, the use of Bioglass® 45S5 and other bioactive glasses for bone engineering applications has been limited due to their relatively poor mechanical properties.[6]

In this context, the development of novel bioactive glass-ceramics is much needed. Glass-ceramics are materials obtained by controlled crystallization of certain glasses.[7] Bioactive glass-ceramics have been developed to improve the mechanical performance of bioactive materials, including Ceravital and A/W,[8,9] or to introduce other interesting properties, such as the machineable glass-ceramic Bioverit.[1] Although

Correspondence to: P. T. de Oliveira, DDS, PhD, Departamento de Morfologia, Estomatologia e Fisiologia, Faculdade de Odontologia de Ribeirão Preto, Universidade de São Paulo, Av. do Café, s/n-14040-904, Ribeirão Preto, São Paulo, Brazil; e-mail: tambasco@usp.br

Contract grant sponsors: National Council of Scientific and Technological Development (*CNPq, Fundo Verde-Amarelo*), State of São Paulo Research Foundation (FAPESP), Federal University of São Carlos, University of São Paulo

glass-ceramics may exhibit improved mechanical properties over glasses, the introduction of some crystalline phases may sharply decrease the bioactivity. The result is that the bioactivity indexes of the current commercial glass-ceramics are much lower than those of bioactive glasses.[10]

In spite of decreasing the kinetics of the apatite layer formation in simulated body fluid (SBF) K9, crystallization does not inhibit its development, even in fully-crystallized glass-ceramics.[11,12] In addition, depending on the characteristics of the crystalline phase that is formed, crystallization provides a temporary good mechanical support.[13] Regarding this important matter, our research group has developed special nucleation and growth thermal treatments to obtain a novel fully crystallized bioactive glass-ceramic of the quaternary P_2O_5–Na_2O–CaO–SiO_2 system (Biosilicate®, patent application WO 2004/074199).[14] Crystallinity significantly changes the fracture characteristics of the glass. Therefore, full crystallization of the material may lead to enhanced mechanical properties of the bulk material or less sharp and abrasive particles when the material is milled to obtain a powder.

The present study aimed to evaluate the surface characteristics and the bioactivity of Biosilicate® and to compare to Bioglass® 45S5 (gold standard) and Biosilicate® parent glass. In addition, using calvaria-derived osteogenic cultures, the following key parameters of *in vitro* osteogenesis were assayed: (1) cell morphology and cytoskeleton organization; (2) immunolocalization of the multifunctional proteins bone sialoprotein (BSP), fibronectin, and osteopontin (OPN); (3) growth curve and cell viability; (4) total protein content and alkaline phosphatase (ALP) activity, and (5) mineralized matrix formation. The results showed that Biosilicate® exhibits a hydroxycarbonateapatite (HCA) layer formation on its surface in SBF-K9 as early as 24 h, which is comparable to the class A bioactive glasses. Furthermore, the enhanced *in vitro* bone-like matrix formation on Biosilicate® suggests that such material is most likely an osteoproductive glass-ceramic. This may indicate that Biosilicate® exhibits a much higher bioactivity level than the current commercial apatite-based glass-ceramics.[10]

MATERIALS AND METHODS

Sample preparation and surface characterization

High purity silica and reagent grade calcium carbonate, sodium carbonate, and sodium phosphate were used to obtain glass compositions: Bioglass® 45S5 and Biosilicate® parent glass. Raw materials were weighed and mixed for 30 min in a polyethylene bottle. Premixed batches were melted in Pt crucible at a temperature range of 1250–1380°C for 3 h in an electric furnace (Rapid Temp 1710 BL, CM Furnaces, Bloomfield, NJ) at the Vitreous Materials Laboratory of the Federal University of São Carlos (São Carlos, SP, Brazil). Samples were cast into a 10 mm × 30 mm cylindrical graphite mold. After annealing at 460°C for 5 h, 3 mm thick glass discs were obtained by cutting the cylinders in diamond-blade. To obtain the fully crystallized Biosilicate® glass-ceramic, Biosilicate® parent glass cylinders underwent cycles of thermal treatment to promote their crystallization. The first thermal cycles were performed at lower temperatures aimed to promote volumetric nucleation of crystals. Afterwards, the nucleated samples were submitted to thermal treatments above the glass transition temperature to lead to a fully crystallized material. The compositions and thermal treatment schedules for obtaining the Biosilicate® glass-ceramic is described in detail in the patent application WO 2004/074199.[14]

The Biosilicate® cylinders were cut into 3 mm thick discs using a diamond-blade. Finally, 12 mm in diameter and 3 mm thick discs were polished with silicon carbide abrasive powder (1000 grit), immersed in isopropyl alcohol, and cleaned by sonication. The discs were then rinsed with and stored in isopropyl alcohol to avoid surface modification by moisture. For the cell culture experiments, the discs were sterilized in dry heat at 180°C for 2 h.

Surface characterization of the Biosilicate® glass-ceramic and the control bioactive glasses was performed by conventional light microscopy, scanning electron microscopy (SEM), and Fourier transform infrared (FTIR) spectroscopy, as described below.

Light microscopy examinations were carried out to confirm the crystallinity of the fully crystallized Biosilicate® and to characterize its microstructure. The discs were polished with silicon carbide powder upto grit 1000 and with a suspension of finer CeO_2. The polished surfaces were treated with 0.5% HF for 5 s, rinsed with water, acetone, and air-dried. The samples were then examined under reflected light using a Leica DMRX light microscope (Leica, Bensheim, Germany), outfitted with a Sony CCD-IRIS digital camera (Sony, Tokyo, Japan).

To simulate the early changes in surface topography and chemistry that cells will interact with and to allow its proper characterization, discs with the same surface preparation used for cell cultures were immersed in supplemented culture medium (see composition described below) in the absence of cells with a ratio of surface area of material to the volume of solution ($R_{SA/VS}$) = 1 cm^{-1} at 37°C in a humidified atmosphere with 5% CO_2. After 12, 24, and 72 h, the discs were briefly washed in distilled water, air-dried, and kept in a desiccator to avoid surface changes by humidity.

The surfaces of randomly-selected Biosilicate® and control discs were examined using a Phillips XL 30 field emission gun scanning electron microscope (Philips, Eindhoven, the Netherlands) operated at 20 kV. Discs stored in isopropyl alcohol (time 0) and exposed to culture conditions in the absence of cells for 12, 24, and 72 h were glued in aluminum sample holders and had their surfaces sputtered with carbon. Micrographs were then taken at different magnifications and processed with the Adobe Photoshop software (version 7.0.1, Adobe Systems).

Bioactivity tests were performed to compare the *in vitro* bioactivity level of the samples in acellular solution using SBF-K9.[15,16] This solution has all the ions found in the human blood plasma in a very similar concentration. Such an assay is universally used for testing bioactive materials, in which the samples rest in the solution usually with $R_{SA/VS} = 0.1$ cm^{-1} and 36.7°C. The discs had their flat surface briefly grounded in water with silicon carbide paper 400 grit and then were immediately rinsed with acetone followed by isopropyl alcohol. After drying, they were immersed in the SBF-K9 solution in a polypropylene flask with impervious sealing.

The surface chemistry was assayed by FTIR spectroscopy in a PerkinElmer Spectrum GX (PerkinElmer Life and Analytical Sciences, Shelton, CT) in reflectance mode. Samples immersed in isopropyl alcohol (time 0) and exposed to the culture conditions in the absence of cells for 12, 24, and 72 h, and to SBF for 24 h were evaluated.

Cell isolation and primary culture of osteogenic cells

Osteogenic cells were isolated by sequential trypsin/collagenase digestion of calvarial bone from newborn (2–4 days) Wistar rats, as previously described.[17–20] All animal procedures were in accordance with guidelines of the Animal Research Ethics Committee of the University of São Paulo. Cells were plated on discs placed in 24-well polystyrene plates at a cell density of 20,000 cells/well. The plated cells were grown for periods up to 17 days using Gibco α-Minimum Essential Medium with L-glutamine (Invitrogen, Carlsbad, CA) supplemented with 10% fetal bovine serum (Invitrogen), 7 m*M* β-glycerophosphate (Sigma, St. Louis, MO), 5 μg/mL ascorbic acid (Sigma), and 50 μg/mL gentamicin (Invitrogen), at 37°C in a humidified atmosphere with 5% CO_2. The culture medium was changed every 3 days. The progression of cultures was examined by phase contrast microscopy of cells grown on polystyrene.

Growth curve and cell viability

Cells grown for periods of 4, 7, and 11 days were enzymatically detached from the culture substrate using 1 m*M* EDTA, 1.3 mg/mL collagenase, and 0.25% trypsin solution (Gibco, Invitrogen). Total number of cells/well, and percentage of viable and nonviable cells were determined after Trypan blue (Sigma) staining using a hemacytometer (Hausser Scientific, Horsham, PA).

Total protein content

Total protein content was determined using a modification of the Lowry method.[21] Briefly, proteins were extracted from each well with 0.1% sodium lauryl sulfate (Sigma) for 30 min and mixed 1:1 with Lowry solution (Sigma) for 20 min at room temperature (RT). The extract was diluted in Folin and Ciocalteau's phenol reagent (Sigma) for 30 min at RT. Absorbance was measured at 680 nm using a spectrophotometer (Cecil CE3021, Cambridge, UK). The total protein content was calculated from a standard curve, and expressed as μg/mL.

ALP activity

ALP activity was assayed in the same lysates used for determining total protein content, as the release of thymolphthalein from thymolphthalein monophosphate using a commercial kit (Labtest Diagnóstica, MG, Brazil). Briefly, 50 μL of thymolphthalein monophosphate was mixed with 0.5 mL of 0.3*M* diethanolamine buffer (pH 10.1), and left for 2 min at 37°C. The solution was then added to 50 μL of the lysates obtained from each well for 10 min at 37°C. For color development, 2 mL of 0.09*M* Na_2CO_3 and 0.25*M* NaOH were added. After 30 min, absorbance was measured at 590 nm, and ALP activity was calculated from a standard curve using thymolphthalein to give a range from 0.012 to 0.4 μmol thymolphthalein/h/mL. Data were expressed as ALP activity normalized for total protein content. Some cultures were also stained with Fast red, as described elsewhere,[22] for histochemical detection of ALP activity during the mineralization phase of the cultures.

Indirect immunofluorescence for localization of noncollagenous bone matrix proteins

At days 1, 3, 5, and 14, cells were fixed for 10 min at RT using 4% paraformaldehyde in 0.1*M* sodium phosphate buffer (PB), pH 7.2. After washing in PB, cultures were processed for immunofluorescence labeling.[20] Briefly, they were permeabilized with 0.5% Triton X-100 in PB for 10 min, followed by blocking with 5% skimmed milk in PB for 30 min. Primary monoclonal antibodies to BSP (anti-BSP 1:200, WVID1-9C5, Developmental Studies Hybridoma Bank, Iowa City, IA), fibronectin (anti-FN 1:100, clone IST-3, Sigma, St. Louis, MO), and OPN (anti-OPN, 1:800, MPIIIB10-1, Developmental Studies Hybridoma Bank) were used, followed by Alexa Fluor 594 (red fluorescence)-conjugated goat anti-mouse secondary antibody (1:200, Molecular Probes, Invitrogen, Eugene, OR) and Alexa Fluor 488 (green fluorescence)-conjugated phalloidin (1:200, Molecular Probes), as a marker of the actin cytoskeleton. Replacement of the primary monoclonal antibody with PB was used as control. All antibody incubations were performed in a humidified environment for 60 min at RT. Between each incubation step, the samples were washed in PB (3 × 5 min). Before mounting for microscope observation, samples were briefly washed with dH_2O and cell nuclei stained with 300 n*M* 4′,6-diamidino-2-phenylindole, dihydrochloride (DAPI, Molecular Probes) for 5 min. Discs were placed face up on glass slides and covered with 12-mm-round glass coverslips (Fisher Scientific, Suwanee, GA) mounted with Prolong antifade (Molecular Probes). The samples were then examined under epifluorescence using a Leica DMLB light microscope (Leica), with N Plan (×10/0.25, ×20/0.40) and HCX PL Fluotar (×40/0.75, ×100/1.3) objectives, outfitted with a Leica DC 300F digital camera, 1.3 Megapixel CCD. The

acquired digital images were processed with Adobe Photoshop software (version 7.0.1, Adobe Systems).

Mineralized bone-like nodule formation

At day 17, cultures were fixed with 4% formaldehyde in PB (pH 7.2) for 2 h at RT. The samples were then washed in the same buffer, dehydrated in a graded series of alcohol, and stained with 2% Alizarin red (Sigma) (pH 4.2), for 8 min at RT. They were photographed with a high-resolution digital camera (Canon EOS Digital Rebel Camera, 6.3 Megapixel CMOS sensor, with a Canon EF 100 mm f/2.8 macro lens) and then also imaged by epifluorescence microscopy. The percentage of the disc area occupied by Alizarin red-stained nodules was determined using the software ImageJ, version 1.34 s (NIH, Bethesda, MD). The amount of calcified matrix was also blind scored by six independent observers, using a scale of absent (0), small (1), moderate (2), and large (3).

Statistical analysis

Where appropriate, comparisons were carried out using the nonparametric Kruskal–Wallis test for independent samples (level of significance: 5%). If the result of the Kruskal–Wallis test was "significant", that is occurrence of at least one significant difference, the Fisher's least significant difference multiple comparisons procedure, computed on ranks rather than data, was performed.[23] The results described below are representative of three sets of primary cultures.

RESULTS

Surface characterization

Light microscopy revealed that no microstructural features were detected for both bioactive glass controls [Fig. 1(A,B)], whereas Biosilicate® exhibited a fully crystallized structure with average crystal size around 5 μm [Fig. 1(C)].

Prior to the cell culture experiments, SEM images showed that all surfaces stored in isopropyl alcohol were flat, exhibiting randomly distributed features created by the polishing and finishing procedures [Fig. 1(D–F)]. After 12 and 24 h under culture conditions in the absence of cells, no relevant changes in surface microtopography except cracks were detected for all surfaces. Most importantly, higher magnification revealed submicron-scale globular structures on Biosilicate® and on control bioactive glasses as early as 12 h [Fig. 1(G–I)].

Despite their different compositions, original samples of Bioglass® 45S5 glass and Biosilicate® parent glass exhibited very similar infrared spectra [Fig. 2(A)]. The only slight difference in the spectra of the control glasses was the shift of the vibrational bands of the Bioglass® 45S5 glass to a lower wavenumber. It is worthy of note that major changes were observed between the spectra of the Biosilicate® parent glass and the fully crystallized Biosilicate®. Figure 2(A) shows that the vibrational band due to Si—O stretch at 1090 cm^{-1} becomes sharper, shifts to 1100 cm^{-1}, and splits into two other vibrational bands at 1140 and 1050 cm^{-1}. Similar changes occurred with the vibrational band at 505 cm^{-1} due to Si—O—Si bend. In the crystalline Biosilicate®, the vibrational band at 505 cm^{-1} splits to vibrational bands at 530 and 460 cm^{-1}. The sharp vibrational band at 620 cm^{-1} of Biosilicate® is probably due to Si—O vibrations.

When submitted to the bioactivity test in SBF-K9 at 36.7°C with $R_{SA/VS} = 0.1$ cm^{-1}, a well-developed layer of HCA formed on all surfaces after 24 h of exposure, detected by the vibrational bands at 600 and 560 cm^{-1} [Fig. 2(B)].

Samples exposed to the cell culture conditions in the absence of cells for 12 h at 37°C with $R_{SA/VS} = 1$ cm^{-1} showed significant changes in the infrared spectra compared to the original surfaces [cf. in Fig. 2, (C) with (A)], with Biosilicate® and the control bioactive glasses exhibiting the same vibrational bands [Fig. 2(C)]. For samples exposed for 24 h to the same culture conditions, the main changes compared to the infrared spectra at 12 h are indicated by arrows in Figure 2(D). They indicate that the vibrational bands at 470 and 800 cm^{-1} decrease and the vibrational band at 590 cm^{-1} increases. The vibrational bands at 800 and 1175 cm^{-1} by 12 h shift slightly to 780 and 1230 cm^{-1} by 24 h, respectively. At 72 h, the composition of the calcium phosphate layer formed is very close to the ones formed at 12 and 24 h. The most significant changes in infrared spectra compared to 24 h are indicated by arrows in Figure 2(E). They indicate that the vibrational bands at 470 and 780 cm^{-1} decrease further and the vibrational band at 590 cm^{-1} increases.

Cell culture experiments

Growth analyses indicated that there were no significant differences in cell number at days 4 and 11, while more cells were adhered on Biosilicate® parent glass at day 7 (Table I). There was no difference in cell viability between Bioglass® 45S5, Biosilicate® parent glass, and Biosilicate® at all time points (Table I). At day 1, phalloidin staining revealed that adherent cells were spread and randomly distributed throughout the surfaces [Fig. 3(A–F)]. On control glass coverslips, cells exhibited fusiform or polygonal shapes [Fig. 3(A)]. Some cells showed typical features of directional cell movement, with leading and trailing edges [Fig. 3(D)]. On such surface, actin cytoskeleton was characterized by bundles of stress fibers

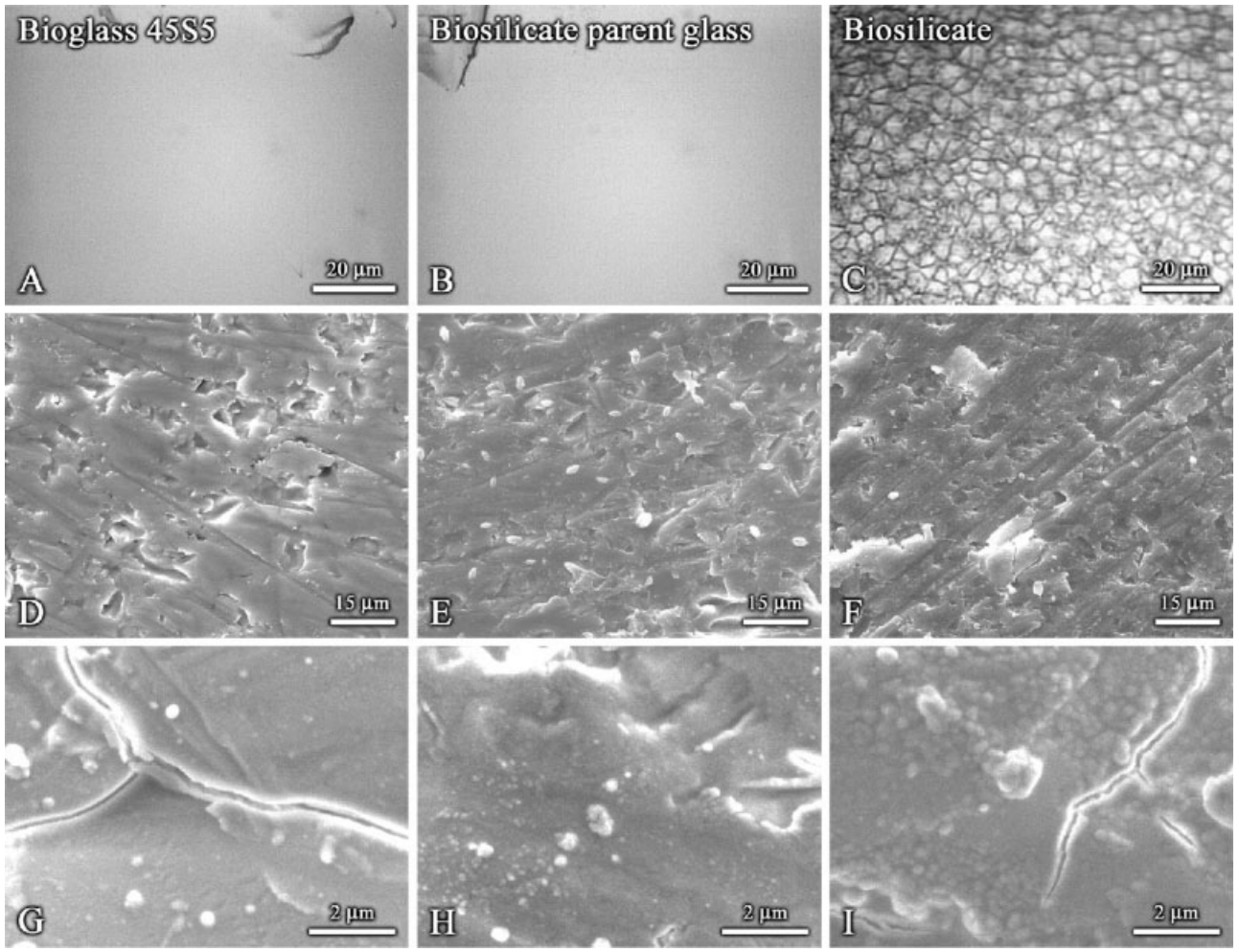

Figure 1. Light microscopy (A–C) and SEM images (D–I) of Biosilicate® glass-ceramic (C, F, I), Bioglass® 45S5 (A, D, G) and Biosilicate® parent glass (B, E, H) surfaces stored in isopropyl alcohol at time 0 (A–F) and exposed to the culture conditions in the absence of cells for 12 h (G–I). While only Biosilicate® exhibits a crystallized surface (cf. C with A and B), all bioactive materials show similar microtopographic features (D–F). After 12 h in culture conditions, submicron-scale globular structures and cracks are noticed on all surfaces (G–I).

throughout the cytoplasm [Fig. 3(D,G,H,K)]. Strikingly, at days 1 and 3, the majority of adherent cells on Biosilicate® and on control bioactive glasses exhibited typical features of actin disassembly, with disruption of stress fibers in varying degrees [Fig. 3(B,C,E,F,I,J,L–N)]. Because of that, cell outlines could not be readily assessed on bioactive surfaces. At day 5, while reassembly/rearrangement of actin stress fibers took place in areas of cell multilayering [Fig. 3(Q,R,T–V)], cells adhering directly to the substrate still exhibited evidences of actin cytoskeleton disruption [Fig. 3(Q,R,T,U)]. Except for glass coverslips, cells with morphological features suggestive of chondrocytic differentiation were occasionally observed in early multilayering nodule formation [Fig. 3(T,U), arrowheads]. Straightforward observation revealed that mitotic figures increased from day 1 to day 5.

At days 1–5, OPN labeling was mainly perinuclear and also detected as punctate deposits throughout the cytoplasm [Fig. 3(A–F,O–R)]. Extracellular OPN accumulations were detected in cultures grown on Biosilicate® [Fig. 3(C,F)], and only occasionally on Bioglass® 45S5 [Fig. 3(B)], in a much lesser extent. Such accumulations were frequently found in association with intensely immunoreactive cells that exhibited morphological features of directional cell movement [Fig. 3(B,C,F)]. No extracellular OPN was evident on Biosilicate® parent glass and on control glass coverslips at any early time points [Fig. 3(A,D)]. At day 3, FN labeling was predominantly localized extracellularly and associated with cell outlines in cultures grown on glass coverslips [Fig. 3(H)]. It is worthy of note that only rarely was FN labeling observed on Biosilicate® [Fig. 3(J)] and on control bioactive glasses [Fig. 3(L)]. At day 5 on all surfaces, cells associated with initial multilayered nodule formation exhibited cytoplasmic OPN labeling [Fig. 3(O–R)]. In addition, only on glass cover-

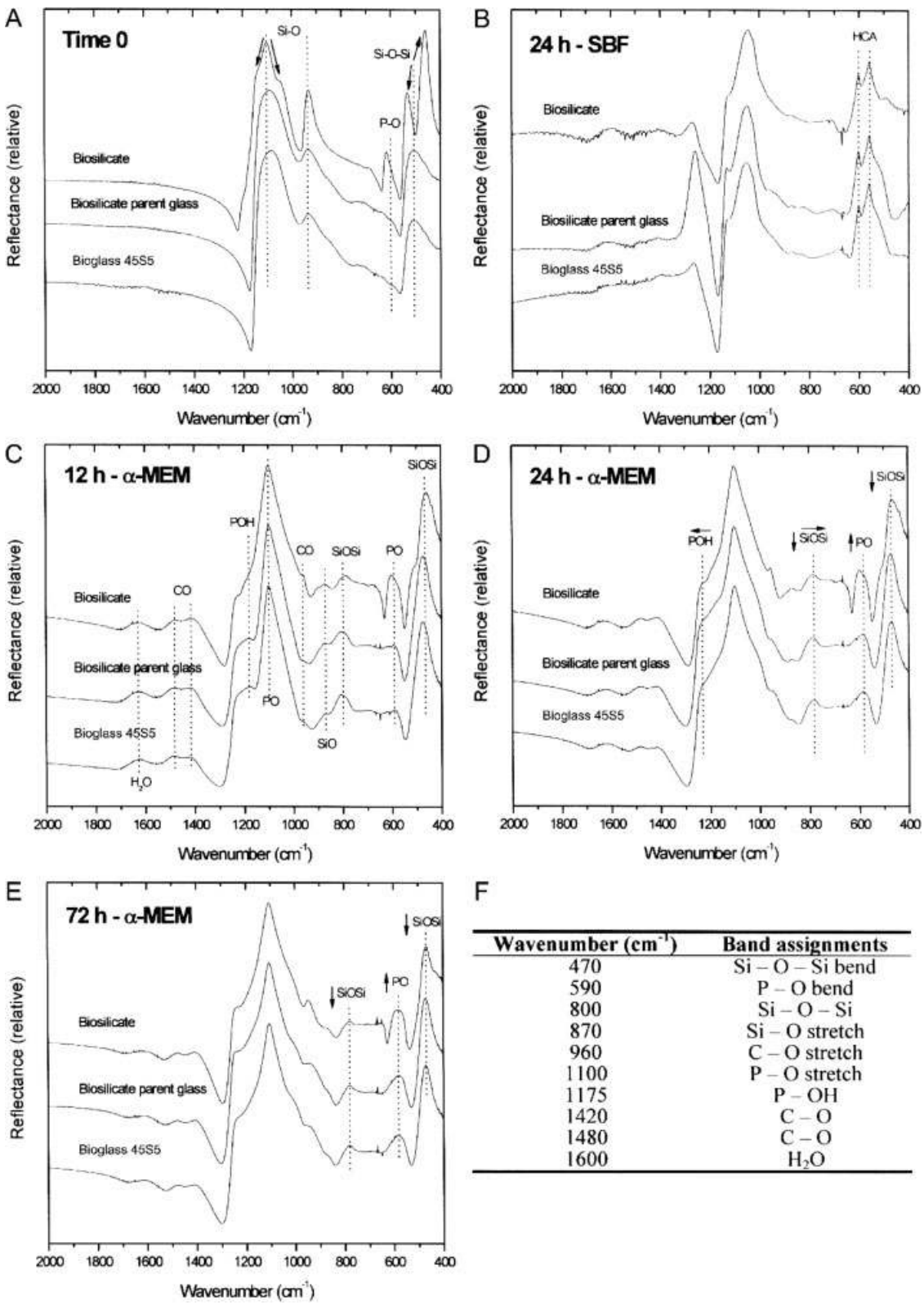

Wavenumber (cm^{-1})	Band assignments
470	Si – O – Si bend
590	P – O bend
800	Si – O – Si
870	Si – O stretch
960	C – O stretch
1100	P – O stretch
1175	P – OH
1420	C – O
1480	C – O
1600	H_2O

Figure 2. FTIR transmission spectra of Biosilicate® glass-ceramic, Bioglass® 45S5, and Biosilicate® parent glass surfaces stored in isopropyl alcohol at time 0 (A), exposed to SBF for 24 h (B), and to the culture conditions in the absence of cells for 12 (C), 24 (D), and 72 h (E). (F) The band assignments and their corresponding wavenumbers.

TABLE I
Quantitative Analysis of Total Cell Number, Cell Viability, Total Protein Content, Alkaline Phosphatase (ALP) Activity, and Alizarin Red-Stained Areas in Osteogenic Cell Cultures Grown on Biosilicate®, and on Control Bioglass® 45S5 and Biosilicate® Parent Glass

Parameters	Time Points (Days)	Bioglass® 45S5	Biosilicate® Parent Glass	Biosilicate®	Kruskal–Wallis Test
Total cell number ($\times 10^4$)	4	5.8 ± 1.5 (4)	8.1 ± 2.4 (4)	7.2 ± 2.2 (4)	NS
	7	21.2 ± 1.9 (4)	35.9 ± 3.3 (4)	22.6 ± 2.6 (4)	S[a]
	11	8.9 ± 2.9 (4)	11.6 ± 3.7 (4)	11 ± 2.3 (4)	NS
Cell viability (%)	4	69.3 ± 7.9 (4)	77.9 ± 5.5 (4)	71 ± 8.2 (4)	NS
	7	81.9 ± 4.7 (4)	79.5 ± 2.2 (4)	78.8 ± 0.7 (4)	NS
	11	73.3 ± 3.1 (4)	65.9 ± 14.7 (4)	71.6 ± 4.6 (4)	NS
Total protein content (μg/mL)	11	153.9 ± 14.5 (5)	140.4 ± 10 (5)	141.4 ± 9.6 (5)	NS
	17	69.4 ± 13.6 (5)	71 ± 13.5 (5)	73.8 ± 9.4 (5)	NS
ALP activity (μmol thymolphthalein/h/mg)	11	13.8 ± 5.4 (5)	19.5 ± 3.2 (5)	15.5 ± 5.9 (5)	NS
	17	5.2 ± 1.5 (5)	6.6 ± 3.3 (5)	5.7 ± 0.8 (5)	NS
Alizarin red-stained areas (scores 0–3)	17	1.5 ± 0.7 (5)	1.3 ± 0.5 (5)	2.5 ± 0.6 (5)	S[b]
Alizarin red-stained areas (%)	17	19.9 ± 16.5 (5)	11 ± 9.3 (5)	50.4 ± 22.2 (5)	S[c]

Data represent mean values ± standard deviation (n). NS, nonsignificant ($p > 0.05$); S, significant ($p < 0.05$).
[a]Multiple comparisons procedure: Bioglass® 45S5 = Biosilicate® ($p > 0.05$); Biosilicate® parent glass > Biosilicate® ($p < 0.01$); Bioglass® 45S5 < Biosilicate® parent glass ($p < 0.01$).
[b]Multiple comparisons procedure: Bioglass® 45S5 < Biosilicate® ($p < 0.05$); Biosilicate® parent glass < Biosilicate® ($p < 0.01$); Bioglass® 45S5 = Biosilicate® parent glass ($p > 0.05$).
[c]Multiple comparisons procedure: Bioglass® 45S5 < Biosilicate® ($p < 0.05$); Biosilicate® parent glass < Biosilicate® ($p < 0.001$); Bioglass® 45S5 = Biosilicate® parent glass ($p > 0.05$).

slips were some cells also labeled for BSP [cf. in Fig 3, (S) with (T–V)]. On bioactive surfaces, BSP-positive cells in areas of cell multilayering were firstly detected at day 7 (not shown).

Total protein content and ALP activity were not affected by substrate either at day 11 or at day 17 (Table I). Higher values for both parameters were observed in cultures grown on all surfaces at day 11, during the onset of matrix mineralization.

For all surfaces, at day 11, epifluorescence microscopy revealed the presence of Fast red-stained cells predominantly in areas of cell multilayering [Fig. 4(A–C)]. At day 14, cells on the surface of mineralized matrix formation exhibited cytoplasmic BSP labeling mainly in the juxtanuclear Golgi area and as punctate deposits [Fig. 4(D–F)]. Extracellular BSP labeling was only rarely detected. Apoptotic bodies were frequently observed during the mineralization phase of cultures grown on all surfaces mainly in areas other than those of bone-like nodule formation [Fig. 4(G–I)]. At day 17, for all surfaces, Alizarin red-stained areas exhibited numerous lacunae, which contained osteocyte-like cells [Fig. 4(J)]. The Alizarin red-stained areas were more abundant on Biosilicate® than on control bioactive glasses [cf. in Fig. 4, (L) with (K)].

Semiquantitative analyses by scores and percentage of surface area of Alizarin red-stained cultures at day 17 revealed significantly larger yellowish/brownish areas of calcified matrix on Biosilicate® than on control bioactive glasses (Biosilicate® >Bioglass® 45S5=Biosilicate® parent glass; Table I, Fig. 5). In addition, surface areas with no macroscopic signs of bone-like matrix formation were reddish in color for all materials (Fig. 5). Control bioactive glasses were originally translucent, whereas Biosilicate® discs were white opaque. Interestingly, using the same culture conditions in the absence of cells, all materials exhibited a reddish surface when stained with Alizarin red at day 7 (not shown).

DISCUSSION

The results of the present study showed that (1) Biosilicate® and the control glasses Bioglass® 45S5, and Biosilicate® parent glass are bioactive materials, based on the formation of an apatite layer in SBF for 24 h, (2) as early as 12 h under culture conditions and in the absence of cells, all surfaces developed a layer of silica-gel that was gradually covered by amorphous calcium phosphate deposits, which remained amorphous up to 72 h, and (3) although all the bioactive materials evaluated supported *in vitro* osteogenesis, significantly larger areas of calcified matrix were detected for the fully crystallized glass-ceramic (Biosilicate®).

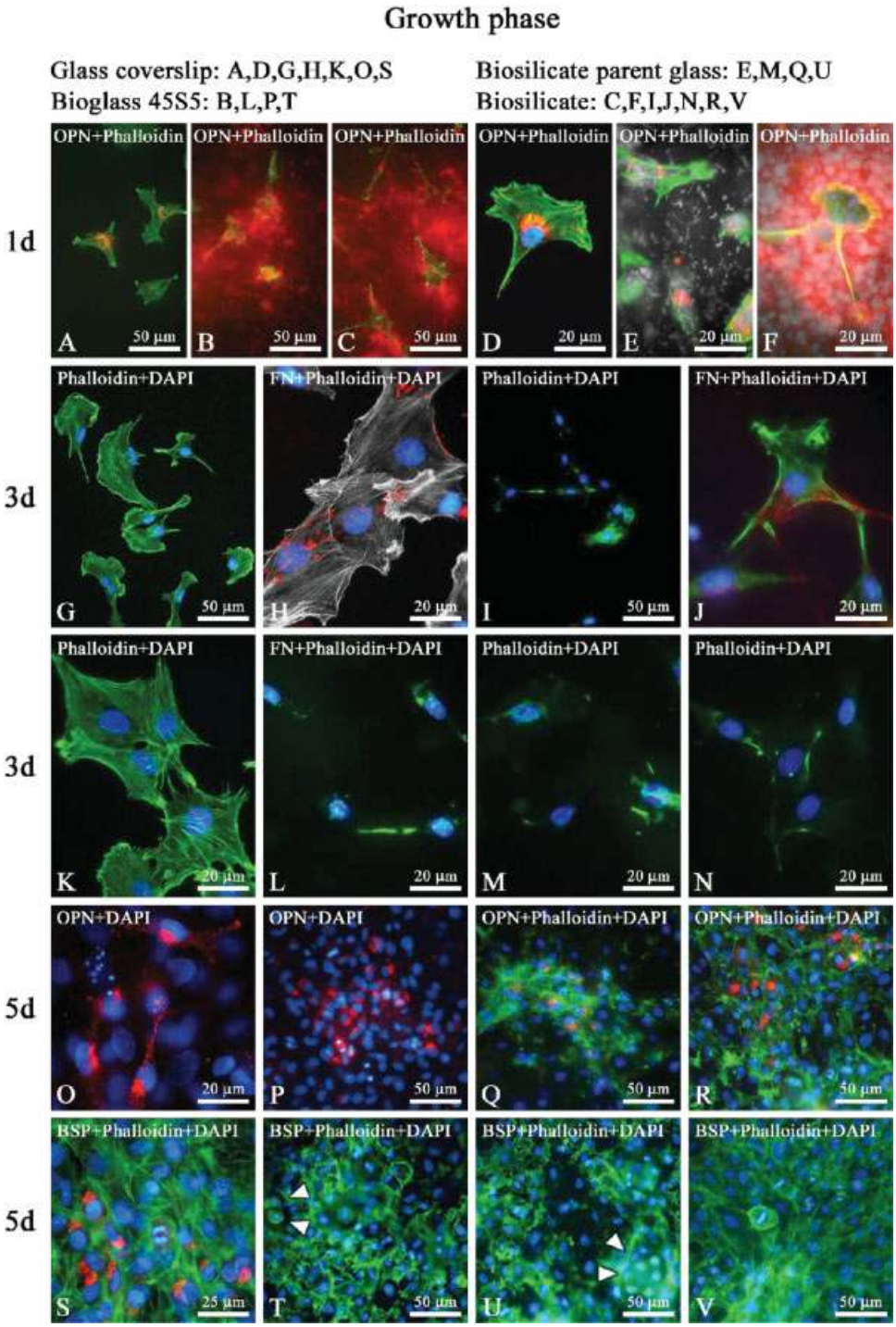

Figure 3. Fluorescence labeling preparations of osteogenic cultures grown on Biosilicate® glass-ceramic (C, F, I, J, N, R, and V), control bioactive glasses Bioglass® 45S5 (B, L, P, and T), and Biosilicate® parent glass (E, M, Q, and U), and control glass coverslips (A, D, G, H, K, O, and S) at days 1 (A–F), 3 (G–N), and 5 (O–V). Green fluorescence (Alexa Fluor 488-conjugated phalloidin) reveals actin cytoskeleton (A–N and Q–V; H in pale white), while blue fluorescence (DAPI DNA stain) highlights cell nuclei (D and G–V). At day 1, the majority of cells on bioactive surfaces exhibit disassembly of actin cytoskeleton, whereas all cells on control glass coverslips show bundles of stress fibers throughout their cytoplasm (cf. B and C with A, and E and F with D). Osteopontin (OPN) labeling (red fluorescence) on control glass coverslips is mainly cytoplasmic, in a region suggestive of the Golgi apparatus (A and D) and in some granules. Noteworthy, on Biosilicate® (C and F) and in a less extent on Bioglass® 45S5 (B), OPN labeling is also characterized by extracellular deposits adjacent to cells exhibiting strong cytoplasmic labeling and typical morphology of directional cell movement. At day 3, almost all cells on bioactive surfaces exhibit a significant decrease in actin labeling, suggestive of disruption of stress fibers, while cells on glass coverslips appear more spread, showing bundles of stress fibers (cf. I with G, and L–N with K). Fibronectin (FN) labeling (red fluorescence) is predominantly extracellular and associated with cell outlines for cultures grown on glass coverslips (H). Conversely, FN labeling is only rarely detected in cultures grown on bioactive surfaces (J and L). At day 5, reassembly of actin cytoskeleton takes place in areas of cell multilayering on all bioactive surfaces (Q, R, and T–V). OPN labeling is detected on all surfaces (O–R), whereas bone sialoprotein (BSP) labeling (red fluorescence) is only detected on glass coverslips (cf. T–V with S). Focal areas of group of cells exhibiting typical aspects of chondrocytic differentiation are observed on control bioactive surfaces (T and U, arrowheads) and on Biosilicate®. [Color figure can be viewed in the online issue, which is available at www.interscience.wiley.com.]

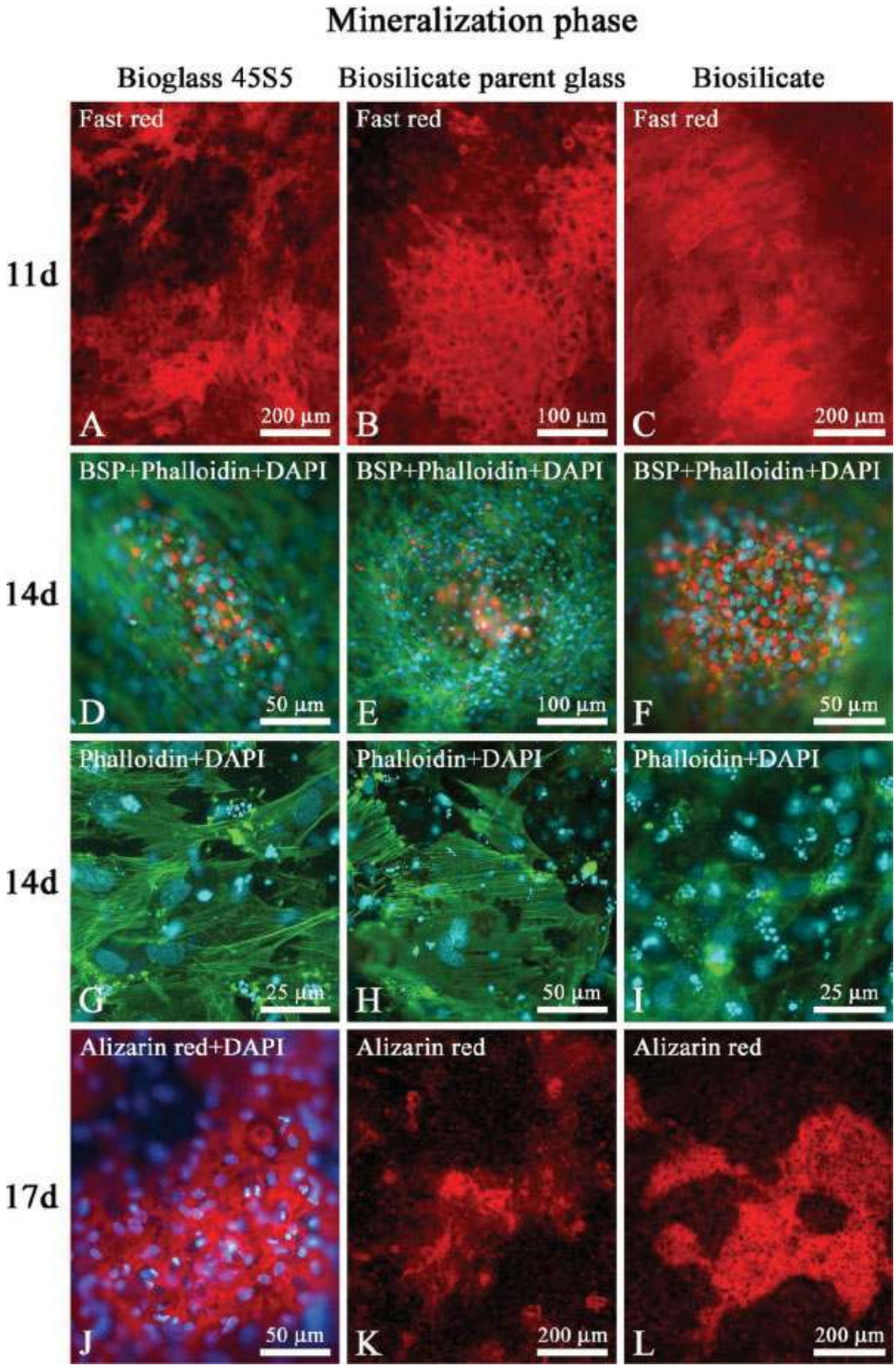

Figure 4. Epifluorescence of osteogenic cultures grown on Biosilicate® glass-ceramic (C, F, I, and L), on control bioactive glasses Bioglass® 45S5 (A, D, G, and J), and Biosilicate® parent glass (B, E, H, and K) at days 11 (A–C), 14 (D–I), and 17 (J–L). At day 11, nodular areas on all surfaces exhibit ALP activity, as revealed by Fast red staining (A–C). At day 14, BSP labeling (red fluorescence) is predominantly detected within the cells in nodular areas on Biosilicate® (F) and on control bioactive glasses (D and E). In areas of cell monolayer, large amounts of apoptotic bodies are observed on all bioactive surfaces (G–I). At day 17, Alizarin red-stained areas exhibit lacunae containing osteocyte-like cells (J). Noteworthy, larger areas of calcified matrix are observed on Biosilicate® (cf. L with K). Green fluorescence (Alexa Fluor 488-conjugated phalloidin) reveals actin cytoskeleton (D–I), while blue fluorescence (DAPI DNA stain) highlights cell nuclei (D–J). [Color figure can be viewed in the online issue, which is available at www.interscience.wiley.com.]

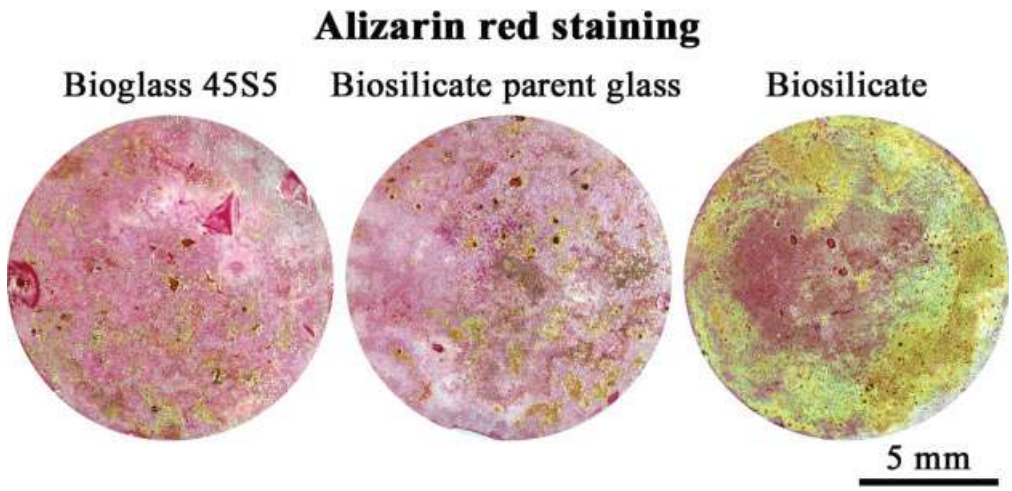

Figure 5. Macroscopic images of osteogenic cultures grown on Biosilicate® glass-ceramic, on control bioactive glasses Bioglass® 45S5, and Biosilicate® parent glass, stained with Alizarin red at day 17. Biosilicate® supports larger amounts of bone-like matrix formation (yellowish areas in a reddish background). [Color figure can be viewed in the online issue, which is available at www.interscience.wiley.com.]

It has been generally agreed that surface topography and chemistry are key factors to control tissue-implant interactions. In the present study, surface topography was qualitatively evaluated by light microscopy (reflected light) and SEM, whereas surface chemistry was analyzed by FTIR. While only Biosilicate® exhibited a fully crystallized surface, no relevant changes in topographic features due to surface preparation were detected for all surfaces stored in isopropyl alcohol. Concerning chemical composition, the Biosilicate® glass-ceramic, the control bioactive glasses Bioglass® 45S5, and Biosilicate® parent glass belong to the quaternary P_2O_5–Na_2O–CaO–SiO_2 system. Although no major changes in terms of FTIR spectra were detected between both glass controls, the vibrational bands of Bioglass® 45S5 was slightly shifted to smaller wavenumbers. Indeed, the increase of the modifiers Na^+ and Ca^{2+} causes a shift of the vibrational bands of SiO_2 towards smaller wavenumbers, resulting from the depolimerization of the silicate framework of the glass. These shifts have already been demonstrated for other glass systems[24] and support the fact that Biosilicate® parent glass presents reduced concentration of glass modifiers compared to Bioglass® 45S5. The FTIR spectrum for Biosilicate® was significantly different from both control glasses. In glasses above the glass transition temperature, the covalent bond angles have some freedom to vary in a small range within the random network. The resulting infrared spectrum of the material is a sum of the contributions of the vibrations in this range. Conversely, in crystallized materials the bonding angles and lengths are well defined, which account for the original vibrational bands of the glass to split, shift, and sharpen in the spectrum of the crystallized material, as observed for Biosilicate®.

The bioactivity of Biosilicate® and of the control Bioglass® 45S5, and Biosilicate® parent glass (i.e., the bone-bonding ability of such materials) was assayed according to the ability of HCA to form on their surfaces in SBF with ion concentrations nearly equal to those of human blood plasma.[16] FTIR revealed that all materials developed a HCA layer formation after 24 h in SBF-K9 at 36.7°C with $R_{SA/VS} = 0.1$ cm^{-1} and that full crystallization did not alter such layer formation. However, when the materials were exposed to the culture conditions in the absence of cells, with $R_{SA/VS} = 1$ cm^{-1}, only silica-gel and calcium phosphate deposits with no crystallization were detected at 12, 24, and 72 h, with a progressive reduction of silica-gel and increase of the phosphate-related vibrational bands. Such results were supported by the SEM observation of a globular surface pattern at the submicron scale on all surfaces as early as 12 h, suggestive of precipitated amorphous calcium-phosphate onto the silica-gel layer, representing the *in vitro* surface reaction stages 3 and 4 of class A bioactive materials.[2,3,25] That the silica-gel layer was formed was revealed by both SEM and FTIR analyses, by the presence of surface cracks due to the shrinkage of the fragile silica-gel layer during fast drying of the samples and the vibrational bands at 470, 800, and 870 cm^{-1}, respectively. The differences in the kinetics of the surface reactions for samples exposed to the culture medium compared to the ones exposed to SBF-K9 could be attributed not only to the solution itself, with diverse ionic concentrations and the presence of other substances and pH conditions, but also to variations in the ratio $R_{SA/VS}$. The latter may affect the pH of the solution, the rate of dissolution of the material, the saturation of the solution with the released ions, and

the concentration of ions necessary to the HCA formation by total consumption. Finally, the possibility that molecules in the culture medium could inhibit crystal nucleation and HCA layer formation should not be ruled out. Irrespective of the exact mechanism, the slower surface reactions under the culture conditions would result in interactions of the cells with the reactive surface over a longer period of time.

The *in vitro* five-stage surface reactions of class A bioactive materials have been described to alter the gene expression profile of osteoblast lineage cells through the release of ionic products and the generation of an alkaline pH at the material surface, promoting osteoblast differentiation and function.[1,3,4,26,27] In addition, surface reactions most likely affect early interactions of cells with matrix/serum proteins and substrate topography and chemistry, such as cell adhesion, spreading, and protein adsorption, which have also been demonstrated to influence interfacial tissue formation.[2,28,29] In the present study, all bioactive surfaces affected actin cytoskeleton assembly as early as 24 h post-plating, resulting in disruption of actin stress fibers with a significant reduction in phalloidin labeling. Remarkably, cell-mediated fibronectin fibrillogenesis was also significantly reduced on such surfaces, compared to control glass coverslips, where cells exhibited well-developed actin stress fibers and an associated fibronectin fibrillar matrix. It is generally agreed that surface effects on cells are often mediated through integrins that bind the Arg–Gly–Asp (RGD) sequence of cell adhesion-associated serum/matrix proteins.[30] Moreover, it has been demonstrated that the assembly of F-actin depends on integrin binding to RGD sequence and focal adhesion assembly,[31] and that the tension generated by the actin cytoskeleton contributes to the assembly of a fibronectin fibrillar matrix.[32–34] This could explain the differences observed in fibronectin labeling between bioactive and bioinert surfaces. Actin disassembly has already been demonstrated in cells grown on smooth and rough 45S5 monoliths at early time points, and the maintenance of such phenotype on rough surfaces has been associated with eventual enhanced bone nodule formation.[29] Because the dynamics in actin assembly/disassembly were similar for Biosilicate® and control bioactive glasses, such biologic process could not explain the differences noticed between surfaces in terms of amount of bone formation. In our study, reassembly of stress fibers took place in areas of initial cell multilayering by day 5 on all bioactive surfaces. In addition, F-actin-associated fibronectin matrix assembly also took place in such areas (not shown), consistent with the fact that fibronectin is essential for osteoblast differentiation and bone-like nodule formation *in vitro*.[35,36]

Biomaterial surfaces, including those of bioactive glasses, have been coated with RGD peptides aiming to improve initial cell-substrate interactions.[37,38] Early matrix deposition of OPN, a RGD-containing matricellular protein, among other serum/matrix molecules, has been considered a key event in the development of the bone–material interface.[39–41] In the present study, initial secretion of OPN took place mainly for cultures grown on Biosilicate® and was associated with cells exhibiting typical morphological aspects of directional cell movement. Enhanced extracellular accumulations of OPN has been observed at early time points in calvaria-derived osteogenic cultures grown on bioactive nanostructured titanium surfaces,[20] which eventually support increased bone-like nodule formation compared to machined surfaces.[42] Such biologic event should be taken into consideration in strategies to design novel biomaterial surfaces modified with bioactive peptides/proteins with cell adhesion capacity.

Parameters to evaluate quantitatively the growth and differentiation phases of the primary osteogenic cultures did not show any relevant differences between the bioactive materials tested. Noteworthy, despite such results, the total area of bone-like formation was enhanced for Biosilicate®, as detected histochemically. Because the pattern of matrix mineralization prevented accurate quantification of calcified areas, bone-like formation at day 17 was evaluated by two different semiquantitative methods. Both analyses by scores and percentage of surface area stained with Alizarin red revealed significantly larger areas of calcified matrix on Biosilicate® than on control bioactive glasses. Trypsin/collagenase digestion of newborn rat calvarial bone allows the isolation of a mixed, heterogeneous cell population composed of osteoprogenitors, preosteoblasts, differentiated osteoblasts, osteocytes, and fibroblasts.[17,19,43,44] Under the osteogenic conditions used in this study, calvaria-derived primary cultures generate woven bone-like nodules, which have been demonstrated to derive from the clonal expansion of osteoprogenitors and their entry into the osteoblast differentiation sequence.[17,43–45] The role of isolated active osteoblasts in the process of matrix mineralization *in vitro* is still unclear.[19,46] The rate of bone formation will mostly be determined by the rate of replication of osteoprogenitors, the number of active osteoblasts, and their life-span.[47,48] Additionally, the enhanced production of bone-like matrix by osteogenic cells grown on Biosilicate® could result from the selective recruitment of progenitor cells from the mixed cell population obtained following enzymatic digestion of calvarial bone and the stimulation of osteoblast activity by ionic products distinctively released from Biosilicate® into the culture medium. For all bioactive surfaces, areas of fibroblastic cell monolayer with no microscopic signs of matrix mineralization

exhibited large amounts of apoptotic cells, which has also been described for Bioglass® 45S5.[3]

Bioglass® 45S5 and Biosilicate® parent glass have a homogeneous glass matrix and the concentration of each chemical element is supposed to be uniform all over the material, thus the dissolution rate is the same all over the surface. On the other hand, during the crystallization process of Biosilicate®, selective attachment of atoms on the crystal growth front may occur, resulting in the production of a chemical gradient from the crystal centre to its border. Indeed, during crystallization of glasses of the Na_2O–CaO–SiO_2 system having compositions close to the stoichiometric Na_2O–2CaO–$3SiO_2$, Fokin et al.[49,50] provided strong evidence for a continuous variation in both glass and crystal compositions. Partially crystallized samples show Na-enriched crystals, compared to the glassy matrix, while the glassy matrix exhibit a slightly higher concentration of Ca. The authors attributed the occurrence of such phenomenon to the measured variations of crystal growth velocity, nucleation rate, crystal lattice parameters, and other properties with increasing degree of crystallization. Similarly, the centre of each crystal in Biosilicate® could be enriched in Na, while its border would be depleted. The concentration of Ca would then vary in the opposite direction. In the first step of HCA formation on bioactive glasses of this family, there is an exchange of Na^+ of the glass surface with H^+ of the solution. If the above described compositional variations really occur, this exchange reaction would then take place near the crystal border with a slower rate compared to the parent glass. Therefore, the local pH increase would be higher near each crystal centre than on its border, causing the breakage of Si—O—Si bonds and release of $Si(OH)_4$ in the solution at a higher rate in the central region. Thus, despite their identical (average) chemical composition, Biosilicate® and its parent glass may have different kinetics of dissolution depending on each specific region of the interface with bone tissue. Even if the overall surface concentration of Na in both materials is the same, primary calvarial cells could be sensitive to the Na enriched surface spots and their local pH, which would catalyze the release of ionic products in the solution that are known to regulate osteoblast differentiation and function.[3–5] Such phenomenon gives a preliminary explanation for the different results observed on bone-like tissue formation for the fully crystallized Biosilicate® glass-ceramic compared to the control Bioglass® 45S5 and Biosilicate® parent glass surfaces.

CONCLUSIONS

We have demonstrated that the strategy used to improve the mechanical performance of the Biosilicate® parent glass by crystallization may also alter other important properties of the material, such as the dissolution rate. Although no major differences between all bioactive materials tested have been observed during the growth and differentiation phases of primary osteogenic cultures, the fully crystallized Biosilicate® glass-ceramic supported a significant enhancement of calcified tissue areas. The remarkable early changes in actin cytoskeleton and fibronectin matrix assemblies are most likely determined by the dynamic changes that take place on the reactive bioactive glass/glass-ceramic surfaces, and therefore could not explain the difference between Biosilicate® and the control bioactive glasses in terms of amount of bone-like tissue formation. The results presented herein open the doors for the development of a novel bioactive scaffold for bone tissue engineering applications.

The authors thank Roger Rodrigo Fernandes and Júnia Ramos for technical assistance. The mouse monoclonal anti-rat osteopontin (MPIIIB10-1) and anti-rat bone sialoprotein (WVID1-9C5) antibodies, developed by Michael Solursh and Ahnders Franzen, were obtained from the Developmental Studies Hybridoma Bank formed under the auspices of the NICHD and maintained by Department of Biological Sciences, The University of Iowa (Iowa City, IA 52242). Lucas Novaes Teixeira was the recipient of an internship scholarship from CNPq.

References

1. Hench LL, Wilson J. An introduction to bioceramics. Singapore:World Scientific; 1993. 386 pp.
2. Ducheyne P, Qiu Q. Bioactive ceramics: The effect of surface reactivity on bone formation and bone cell function. Biomaterials 1999;20:2287–2303.
3. Hench LL, Polak JM, Xynos ID, Buttery LDK. Bioactive materials to control cell cycle. Mat Res Innov 2000;3:313–323.
4. Xynos ID, Edgar AJ, Buttery LD, Hench LL, Polak JM. Gene-expression profiling of human osteoblasts following treatment with the ionic products of Bioglass 45S5 dissolution. J Biomed Mater Res 2001;55:151–157.
5. Hench LL, Polak JM. Third-generation biomedical materials. Science 2002;295:1014–1017.
6. Dieudonne SC, van den Dolder J, de Ruijter JE, Paldan H, Peltola T, van't Hof MA, Happonen RP, Jansen JA. Osteoblast differentiation of bone marrow stromal cells cultured on silica gel and sol-gel-derived titania. Biomaterials 2002;23:3041–3051.
7. James PF. Glass ceramics: New compositions and uses. J Non-Cryst Solids 1995;181:1–15.
8. Brömer H, Kaes HH, Pfeil E(to ERNST LEITZ GmbH). Biocompatible glass ceramic material. US Patent Documents No. 3,981,736, 21 Sep. 1976. Int. C. A61F001/00.
9. Kokubo T, Ito S, Shigematsu M, Yamamuro T. Mechanical properties of a new type of apatite-containing glass-ceramic for prosthetic application. J Mater Sci 1985;20:2001–2004.
10. Hench LL, West JK. Biological applications of bioactive glasses. Life Chem Rep 1996;13:187–241.
11. Peitl Filho O, LaTorre GP, Hench LL. Effect of crystallization on apatite-layer formation of bioactive glass 45S5. J Biomed Mater Res 1996;30:509–514.

12. Peitl O, Zanotto ED, Hench LL. Highly bioactive P_2O_5-Na_2O-CaO-SiO_2 glass-ceramics. J Non-Cryst Solids 2001;292:115–126.
13. Chen QZ, Thompson ID, Boccaccini AR. 45S5 Bioglass((R))-derived glass-ceramic scaffolds for bone tissue engineering. Biomaterials 2006;27:2414–2425.
14. Zanotto ED, Ravagnani C, Peitl O, Panzeri H, Lara EH. Process and compositions for preparing particulate, bioactive or resorbable biosilicates for use in the treatment of oral ailments, WO2004/074199, Fundação Universidade Federal De São Carlos; Universidade De São Paulo, 20 Feb. 2004, Int. C. C03C10/00.
15. Kokubo T, Kushitani H, Sakka S, Kitsugi T, Yamamuro T. Solutions able to reproduce in vivo surface-structure changes in bioactive glass-ceramic A-W. J Biomed Mater Res 1990;24:721–734.
16. Kokubo T, Takadama H. How useful is SBF in predicting in vivo bone bioactivity? Biomaterials 2006;27:2907–2915.
17. Nanci A, Zalzal S, Gotoh Y, McKee MD. Ultrastructural characterization and immunolocalization of osteopontin in rat calvarial osteoblast primary cultures. Microsc Res Tech 1996;33:214–231.
18. Irie K, Zalzal S, Ozawa H, McKee MD, Nanci A. Morphological and immunocytochemical characterization of primary osteogenic cell cultures derived from fetal rat cranial tissue. Anat Rec 1998;252:554–567.
19. De Oliveira PT, Zalzal SF, Irie K, Nanci A. Early expression of bone matrix proteins in osteogenic cell cultures. J Histochem Cytochem 2003;51:633–641.
20. De Oliveira PT, Nanci A. Nanotexturing of titanium-based surfaces upregulates expression of bone sialoprotein and osteopontin by cultured osteogenic cells. Biomaterials 2004;25:403–413.
21. Lowry OH, Rosebrough NJ, Farr AL, Randall RJ. Protein measurement with the Folin phenol reagent. J Biol Chem 1951;193:265–275.
22. Majors AK, Boehm CA, Nitto H, Midura RJ, Muschler GF. Characterization of human bone marrow stromal cells with respect to osteoblastic differentiation. J Orthop Res 1997;15:546–557.
23. Conover WJ. Some methods based on ranks. In: Conover WJ, editor. Practical nonparametric statistics, 2nd ed. New York: Wiley; 1980. p 213–343.
24. Stoch L, Sroda M. Infrared spectroscopy in the investigation of oxide glasses structure. J Mol Struct 1999;511/512:77–84.
25. Saravanapavan P, Jones JR, Pryce RS, Hench LL. Bioactivity of gel-glass powders in the CaO–SiO_2 system: A comparison with ternary (CaO-P_2O_5-SiO_2) and quaternary glasses (SiO_2-CaO-P_2O_5-Na_2O). J Biomed Mater Res A 2003;66:110–119.
26. Xynos ID, Edgar AJ, Buttery LD, Hench LL, Polak JM. Ionic products of bioactive glass dissolution increase proliferation of human osteoblasts and induce insulin-like growth factor II mRNA expression and protein synthesis. Biochem Biophys Res Commun 2000;276:461–465.
27. Loty C, Sautier JM, Tan MT, Oboeuf M, Jallot E, Boulekbache H, Greenspan D, Forest N. Bioactive glass stimulates in vitro osteoblast differentiation and creates a favorable template for bone tissue formation. J Bone Miner Res 2001;16:231–239.
28. Rosengren A, Oscarsson S, Mazzocchi M, Krajewski A, Ravaglioli A. Protein adsorption onto two bioactive glass-ceramics. Biomaterials 2003;24:147–155.
29. Gough JE, Notingher I, Hench LL. Osteoblast attachment and mineralized nodule formation on rough and smooth 45S5 bioactive glass monoliths. J Biomed Mater Res A 2004;68:640–650.
30. Tosatti S, Schwartz Z, Campbell C, Cochran DL, VandeVondele S, Hubbell JA, Denzer A, Simpson J, Wieland M, Lohmann CH, Textor M, Boyan BD. RGD-containing peptide GCRGYGRGDSPG reduces enhancement of osteoblast differentiation by poly(l-lysine)-graft-poly(ethylene glycol)-coated titanium surfaces. J Biomed Mater Res A 2004;68:458–472.
31. Blystone SD. Integrating an integrin: A direct route to actin. Biochim Biophys Acta 2004;1692:47–54.
32. Schoenwaelder SM, Burridge K. Bidirectional signaling between the cytoskeleton and integrins. Curr Opin Cell Biol 1999;11:274–286.
33. Hynes RO. The dynamic dialogue between cells and matrices: Implications of fibronectin's elasticity. Proc Natl Acad Sci USA 1999;96:2588–2590.
34. Pompe T, Renner L, Werner C. Nanoscale features of fibronectin fibrillogenesis depend on protein-substrate interaction and cytoskeleton structure. Biophys J 2005;88:527–534.
35. Moursi AM, Damsky CH, Lull J, Zimmerman D, Doty SB, Aota S, Globus RK. Fibronectin regulates calvarial osteoblast differentiation. J Cell Sci 1996;109:1369–1380.
36. Moursi AM, Globus RK, Damsky CH. Interactions between integrin receptors and fibronectin are required for calvarial osteoblast differentiation in vitro. J Cell Sci 1997;110:2187–2196.
37. Dee KC, Rueger DC, Andersen TT, Bizios R. Conditions which promote mineralization at the bone-implant interface: A model in vitro study. Biomaterials 1996;17:209–215.
38. Siebers MC, ter Brugge PJ, Walboomers XF, Jansen JA. Integrins as linker proteins between osteoblasts and bone replacing materials. A critical review. Biomaterials 2005;26:137–146.
39. Puleo DA, Nanci. A. Understanding and controlling the bone-implant interface. Biomaterials 1999;20:2311–2321.
40. Nanci A, Zalzal S, Gotoh Y, McKee MD. Ultrastructural characterization and immunolocalization of osteopontin in rat calvarial osteoblast primary cultures. Microsc Res Tech 1996;33:214–231.
41. Davies JE. In vitro modeling of the bone/implant interface. Anat Rec 1996;245:426–445.
42. De Oliveira PT, Zalzal SF, Beloti MM, Rosa AL, Nanci A. Enhancement of in vitro osteogenesis on titanium by chemically produced nanotopography. J Biomed Mater Res A 2006; Epub ahead of print. http://dx.doi.org/10.1002/jbm.a.30955.
43. Bellows CG, Aubin JE, Heersche JNM, Antosz ME. Mineralized bone nodules formed in vitro from enzymatically released rat calvaria cell populations. Calcif Tissue Int 1986;38:143–154.
44. Aubin JE. Advances in the osteoblast lineage. Biochem Cell Biol 1998;76:899–910.
45. Bellows CG, Aubin JE. Determination of numbers of osteoprogenitors present in isolated fetal rat calvaria cells in vitro. Dev Biol 1989;133:8–13.
46. Malaval L, Liu F, Roche P, Aubin JE. Kinetics of osteoprogenitor proliferation and osteoblast differentiation in vitro. J Cell Biochem 1999;74:616–627.
47. Jilka RL, Weinstein RS, Bellido T, Parfitt AM, Manolagas SC. Osteoblast programmed cell death (apoptosis): Modulation by growth factors and cytokines. J Bone Miner Res 1998;13:793–802.
48. Jilka RL, Weinstein RS, Bellido T, Roberson P, Parfitt AM, Manolagas SC. Increased bone formation by prevention of osteoblast apoptosis with parathyroid hormone. J Clin Invest 1999;104:439–446.
49. Fokin VM, Potapov OV, Chinaglia CR, Zanotto ED. The effect of pre-existing crystals on the crystallization kinetics of a soda-lime-silica glass. The courtyard phenomenon. J Non-Cryst Solids 1999;258:180–186.
50. Fokin VM, Potapov OV, Zanotto ED, Spiandorello FM, Ugolkov VL, Pevzner BZ. Mutant crystals in $Na_2O{\cdot}2CaO{\cdot}3SiO_2$ glasses. J Non-Cryst Solids 2003;331:240–253.